PERGAMON

International Journal of Heat and Mass Transfer 42 (1999) 1541–1553

International Journal of HEAT and MASS TRANSFER

An experimental study of flow and heat transfer in sinusoidal wavy passages

T.A. Rush, T.A. Newell*, A.M. Jacobi

Department of Mechanical and Industrial Engineering, University of Illinois at Urbana-Champaign, 1206 W. Green St., Urbana, IL 61801, U.S.A.

Received 3 April 1998; in final form 14 August 1998

Abstract

Local heat transfer and flow behavior are investigated for laminar and transitional flows in sinusoidal wavy passages. The experimental geometry consists of a channel with a 10 : 1 aspect ratio bound by two wavy walls. The walls are from 12 to 14 wavelengths long, and the wave amplitude, phase angle, and wall-to-wall spacing are varied during the experiments. Using visualization methods, the flow field is characterized as steady or unsteady, with special attention directed toward detecting the onset of macroscopic mixing in the flow. The location of the onset of mixing is found to depend on the Reynolds number and channel geometry. Instabilities are manifest near the channel exit at low Reynolds numbers ($Re \sim 200$) and move toward the channel entrance as the Reynolds number is increased; the entire channel exhibits unsteady, macroscopic mixing at moderate Reynolds numbers ($Re \sim 800$). The onset of macroscopic mixing is directly linked to significant increases in local heat transfer.

Nomenclature

A amplitude of side-wall of wavy passage (see Fig. 1)
A_{min} minimum free-flow area in channel flow (see Fig. 1)
D_h hydraulic diameter, $4A_{min}/P$
G mass flow rate
h_x local heat transfer coefficient, $q''(x)/(T_s - T_m)$
H_{avg} average separation distance between wavy walls (see Fig. 1)
H_{max} maximum separation distance between wavy walls (see Fig. 1)
H_{min} minimum separation distance between wavy walls (see Fig. 1)
k thermal conductivity of fluid
L spanwise depth of passage
Nu_x local Nusselt Number, $h_x H_{min}/k$
P wetted perimeter in channel flow
q'' wall heat flux
Re Reynolds number, $G/(\mu L) = V_{max} H_{min}/v = VH_{aug}/v$
Re_D Reynolds number based on hydraulic diameter, VD_h/v
T_m local mixed-mean temperature of the air
T_s local surface temperature of channel wall
V average velocity of channel flow
V_{max} velocity at minimum channel free-flow area
x streamwise distance from entrance of wavy passage
x^* dimensionless distance, $x/H_{min}/Re$.

Greek symbols

φ phase shift between sidewalls of wavy passage
λ wavelength of sidewall of wavy passage
μ dynamic viscosity of fluid
v kinematic viscosity of fluid
ρ density of fluid.

1. Introduction

Liquid-to-air and two-phase-to-air heat exchangers are used in a broad array of thermal management and process applications. In these systems, the air-side heat transfer resistance of the heat exchanger is usually much larger than the liquid or two-phase resistance. For this reason, a range of air-side enhancements is used to improve heat exchanger performance. Most air-side enhancements are based on two main strategies: restarting the thermal

* Corresponding author. Tel.: +1217-333-1655; fax: +1217 333 1942; e-mail: t-newell@uiuc.edu

0017–9310/98/$ - see front matter
PII: S0017–9310(98)00264–6

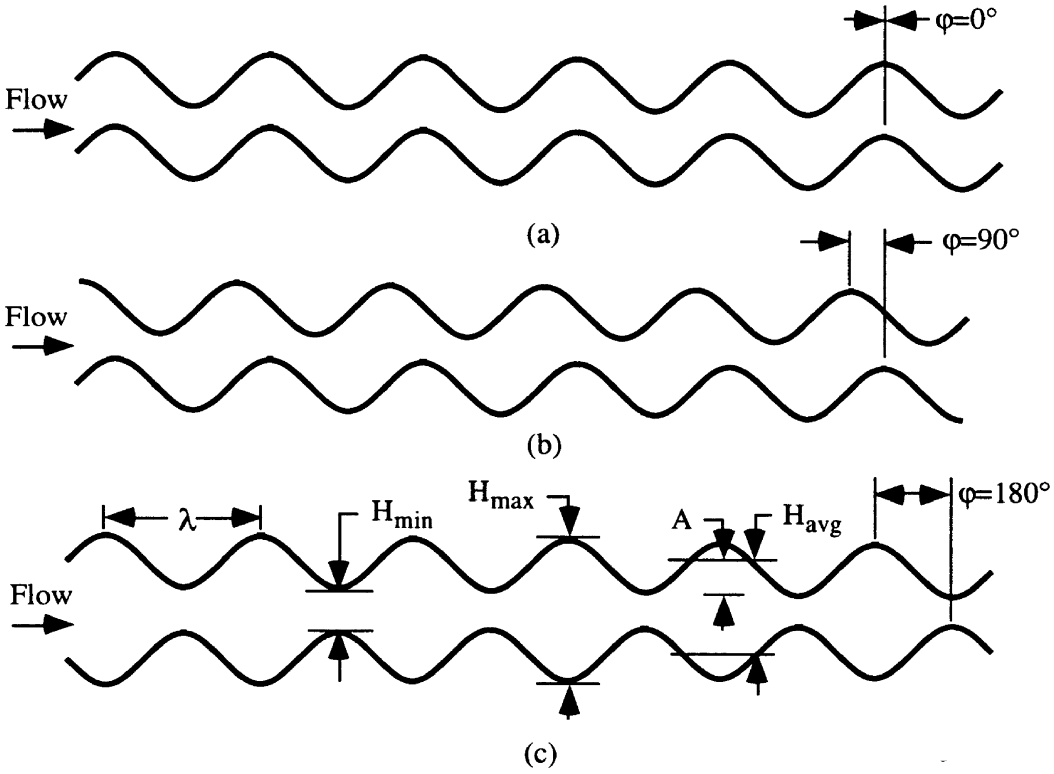

Fig. 1. Schematic of wavy passage configurations and the definition of important geometric parameters (depth of channel is L into page): (a) $\varphi = 0^\circ$ phase shift; (b) $\varphi = 90^\circ$ phase shift; (c) 180° phase shift.

boundary layer and using bulk fluid mixing. Devices such as louvers and offset-strip fins restart the thermal boundary layer and may induce vortices to provide mixing. Destruction and restarting of the boundary layer causes an increase in heat transfer by producing a boundary layer that is thinner on average than the uninterrupted boundary layer. Vorticity in the flow can enhance heat transfer through bulk fluid mixing which reduces temperature gradients in the core flow—concentrating thermal gradients in the near-wall region. Such mixing can be effected using delta-wing vortex generators, surface bumps or other techniques. Jacobi and Shah [1] provide a review and analysis of air-side heat transfer enhancements and discuss these strategies.

The use of wavy fins to enhance air-side heat transfer has been considered for some time; however, researchers have recently revisited this geometry with the hope that the mixing benefits associated with self-sustained unsteadiness might be obtained in wavy passages (see [2] and [3]). An example wavy-fin geometry is shown in Fig. 1. In contrast with louvers and vortex generators, the wavy channel does not use protruding flow manipulators to cause mixing. Instead, mixing in the wavy-channel flow is accomplished through shear-layer instabilities and the formation of spanwise vortices. Exploiting these mechanisms for mixing might lead to improved thermal performance in heat exchanger applications.

As shown in Fig. 1, there are a number of geometric parameters important to characterizing the wavy channel configuration. With a $\varphi = 0^\circ$ phase shift, the two channel walls are in-line with each other, and there is a constant spacing between the channel walls. At the other extreme, the $\varphi = 180^\circ$ phase shift corresponds to the walls being shifted exactly one half wavelength with respect to each other. The cross-sectional area is not constant when the phase shift is nonzero. The following dimensionless variables can be used to characterize flow in channels with sinusoidal wavy walls: phase shift (φ), relative amplitude ($A/H_{\min}$), relative wavelength ($\lambda/H_{\min}$), and Reynolds number (Re).

1.1. Literature survey

A large body of technical literature is available on wavy-channel flow and heat transfer, and thorough reviews have recently become available [2–4]. A survey of the germane literature will be provided to place the current work in context.

Goldstein and Sparrow [5] studied corrugated channels with 'triangular waves'. Although this geometry is some-

what different from sinusoidal waves, many flow features are common to both, and Goldstein and Sparrow were among the first to provide detailed data in this related geometry. Their experiments in laminar, transitional, and turbulent flows used the naphthalene sublimation method and two corrugation cycles (two wavelengths). They concluded that corrugated channels are an effective heat transfer device only at turbulent Reynolds numbers. They found that heat transfer rates improved by a factor of three over a straight channel, but there was an even greater penalty in pumping power. There have been several more experimental and numerical studies of the triangular corrugated geometry [6–11], with the same general conclusions: at low Reynolds numbers there is not much heat transfer enhancement, but at a sufficiently high Reynolds number (generally greater than 1500), there is evidence of flow separation, recirculation, and reattachment with significant heat-transfer enhancements. Unfortunately, there is usually an even greater increase in friction factor.

One way to reduce the pressure drop penalty of the triangular corrugated channel is to round the corners of the channel. For sinusoidal wavy channels with $\varphi = 0^\circ$, a great deal of experimental research has been done by Nishimura and co-workers [12–14]. Using flow visualization techniques, they observed flow separation and recirculation zones in the wave troughs at low Reynolds numbers. As the Reynolds number increased above a critical value (less than 1000), these recirculation zones interacted with the core fluid through a shear-layer instability—near-wall fluid was exchanged with core fluid, and macroscopic mixing occurred. Using mass transfer experiments, Nishimura and co-workers found that interactions between the recirculation zones and core flow lead to an increase in the heat transfer. Using a channel with nine-wavelengths, they concluded that the flow becomes three-dimensional at $Re \sim 100$, with spanwise and streamwise vortices. Asako et al. [15] numerically examined a similar geometry for Re from 100–1000, and they concluded that this geometry had lower friction factors and Nusselt numbers than triangular channels. Heat transfer enhancement was strongly dependent on flow conditions and channel geometry. Later, Garg and Maji [16] numerically investigated $\varphi = 0^\circ$ wavy channels. Their calculations showed the local Nusselt number to be proportional to Re and to vary sinusoidally in the flow direction.

Nishimura et al. [17] also conducted early experimental work on the $\varphi = 180^\circ$ geometry; their study revealed large recirculation zones in the troughs of the channel. These flow structures were much larger than the separation bubbles forming in the 0°-phase-shift geometry. As with the $\varphi = 0^\circ$ geometry, at low Reynolds numbers ($Re < 300$), the core fluid was unaffected by these recirculation zones. At higher Reynolds numbers ($Re \sim 350$), the flow became unsteady as these trapped vortices interacted with the core flow. In later work [18], mass transfer rates were measured and found to increase when the flow became unsteady. The highest local mass transfer occurred where the flow cross-sectional area was a maximum. Nishimura et al. [19] concluded that both $\varphi = 0^\circ$ and $\varphi = 180^\circ$ wavy channels increase mass transfer, but they give rise to markedly different interactions between the recirculation zones and the core flow. Recently, Nishimura et al. [20] studied a sinusoidal wavy channel and a channel comprising a series of circular arcs. For their particular geometry, they concluded that the circular-arc channel undergoes a transition to turbulent flow at a lower Reynolds number than the sinusoidal channel—this behavior corresponded to a mass transfer enhancement.

In recent numerical simulations, Guzmán and Amon [21] solved the conservation equations for a fully developed, two-dimensional flow in a two-wavelength domain using spectral elements. They chose one of the wavy-channel geometries used by Nishimura and co-workers. Their numerical results indicated that the critical Reynolds number for flow separation was about 20. They concluded that the flow becomes chaotic at $Re \sim 750$. The flow was classified into four regimes: laminar, periodic, quasiperiodic, and turbulent. The periodic and quasiperiodic regimes are characterized by self-sustained oscillatory flows with spanwise vortices that form in the troughs of the wavy walls and affect the core flow. Their work has been supported by a more recent three-dimensional study [22]. These numerical studies showed streamlines with the characteristics observed by Nishimura and co-workers; furthermore, the numerical work demonstrated that stable three-dimensional effects do not influence the transitional Reynolds numbers.

Wang and Vanka [23] provided numerical simulations of the $\varphi = 180^\circ$ wavy channel geometry. They solved the full time-dependent, two-dimensional Navier–Stokes equations on a curvilinear grid with periodic boundary conditions. They found the same flow features for this type of geometry that were described earlier. Above a critical Reynolds number of 180, self-sustained oscillations destabilize the laminar momentum and thermal boundary layers and cause an interaction between the near-wall fluid in the troughs of the channel and the core fluid. In this transitional flow regime, the heat transfer was enhanced by a factor of about 2.5, and the friction factor was nearly double that of a flat channel.

A significant body of research on flow and heat transfer in wavy channels is available in the literature (see [2–4] and also [24–26]). However, most work addressing the onset of mixing—whether through laminar unsteadiness or turbulence—considers only fully developed, periodic flows. Results for the onset of mixing in developing wavy channel flows are limited, with no clear characterization of the effects of fin spacing, wave amplitude, wavelength, and phase angle. Nevertheless, in order to properly

exploit the wavy-channel geometry in heat exchanger design, these effects must be understood. The purpose of this paper is to provide flow visualization and heat transfer data that extend the current understanding of developing wavy channel flows. Particular attention is directed toward geometric influences on the onset of macroscopic mixing in the flow, and the impact of macroscopic mixing on local heat transfer.

2. Method

Flow visualization experiments were performed in a water tunnel using twelve different geometries in the laminar flow regime. The experiments revealed the complexity of these flows and disclosed the effects of phase shift (φ), relative wavelength ($\lambda/H_{\min}$), and relative amplitude ($A/H_{\min}$). A wind tunnel was employed to measure the heat transfer in wavy channels, and the experiments were used to associate flow behavior with heat transfer performance.

The closed-loop water tunnel used for the flow visualization experiments is shown schematically in Fig. 2. Most of the water tunnel was constructed using clear acrylic to provide visual access. Upstream of the test section, the flow was conditioned using a honeycomb and screens. Immediately upstream of the test section, the flow passed through a 10 : 1 area contraction designed to provide a uniform, low-turbulence-intensity approach velocity. The volumetric flow rate through the test section was measured to within $\pm 1.5\%$ using a simple bucket and stopwatch technique. Taking geometric and property variations into account, and using standard error analysis techniques, the overall uncertainty in Reynolds number was estimated to be approximately 4.8% (see [4] for details).

A total of twelve test sections were constructed; the geometric parameter space is summarized in Table 1. For $Re < 1000$, experiments were conducted with $\lambda/H_{\min}$ from 2.3–5.6, and with $A/H_{\min}$ from 0.24–0.53, for $\varphi = 0$, 90 and 180°. Each test section was constructed by heating an acrylic to its thermal set point and pressing it into a mold. Channels were constructed to have 12–14 wavelengths. During the experiments, flow in the test section was visualized by injecting dye at the flow contraction—multiple dye streaks were used to provide better visualization. In order to validate the apparatus and methods, a straight test section was initially placed in the water tunnel, and the transitional Reynolds number based on hydraulic diameter was found to be approximately 2500, in agreement with the literature.

The heat transfer experiments were performed in the open-loop wind tunnel, shown schematically in Fig. 3. The mass flow rate was determined by using a smooth,

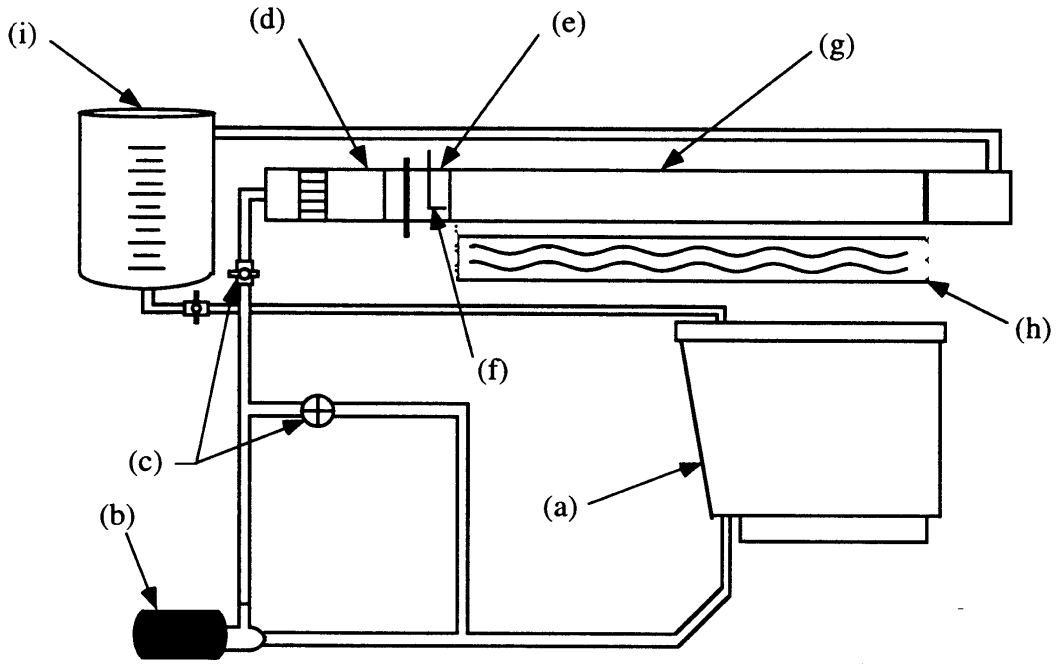

Fig. 2. Schematic of water tunnel used for flow visualization experiments. (a) water reservoir; (b) pump; (c) flow-control valves; (d) flow conditioning section with honeycomb and screens; (e) 10 : 1 area contraction; (f) dye injector; (g) test section; (h) viewing mirror; (i) graduated flow measurement reservoir.

Table 1
Geometric parameter space used in flow visualization experiments

H_{min} (mm)	λ/H_{min}	A/H_{min}	φ (degrees)
12.0	5.6	0.48	180
13.3	5.4	0.47	0
12.4	5.5	0.51	90
11.5	4.8	0.53	180
13.6	4.7	0.47	0
10.3	4.9	0.52	90
23.5	2.4	0.26	180
22.0	2.5	0.26	0
24.0	2.3	0.24	90
23.6	2.9	0.25	180
24.0	2.9	0.25	0
25.0	2.8	0.24	90

30 cm long, drawn copper tube with an inside diameter of 6.9 mm. The pressure drop across the tube was measured with a manometer, and the mass flow rate was calculated using the Colebrook equation [24]. The uncertainty in this measurement was determined using standard methods to be 3.1%. The design of the wind tunnel was similar to that of the water tunnel. The flow was conditioned by a honeycomb and set of screens upstream of test section. The flow passed through a 10 : 1 area contraction into the 10×1 cm flow area of the test section. Upon exiting the test section, the flow was mixed with a series of baffles. The upstream and downstream mixed-mean temperatures were measured with ASTM mercury-in-glass thermometers. The thermometer upstream of the test section had a smallest division of 0.01°C, and the thermometer downstream of the test section had a smallest division of 0.1°C.

The test section walls for heat transfer tests were made by placing a fiberglass cloth with embedded nickel–chromium wires between two thin (0.4 mm thick) corrugated-steel sheets. The outside of the test section was heavily insulated, and the inside walls formed a wavy passage. The walls had a wavelength of 71 mm, an amplitude of 5.7 mm, and the channel length included a total of nine wavelengths. Using this basic geometry, two test sections were constructed: each channel had $\lambda/H_{min} = 5.5$ and $A/H_{min} = 0.50$, but two different phase shifts were tested, $\varphi = 0^\circ$ and $\varphi = 180^\circ$. These test sections were similar to the first two test sections listed in Table 1—the small geometric differences were due to difficulties in manufacturing heat transfer test sections. The power supplied to the nickel–chromium wires was controlled with a variable transformer, allowing a prescribed isoflux boundary condition on the channel walls. Wall temperatures were determined by placing 21 thermocouples, at various axial locations, between the nickel–chromium heater and the

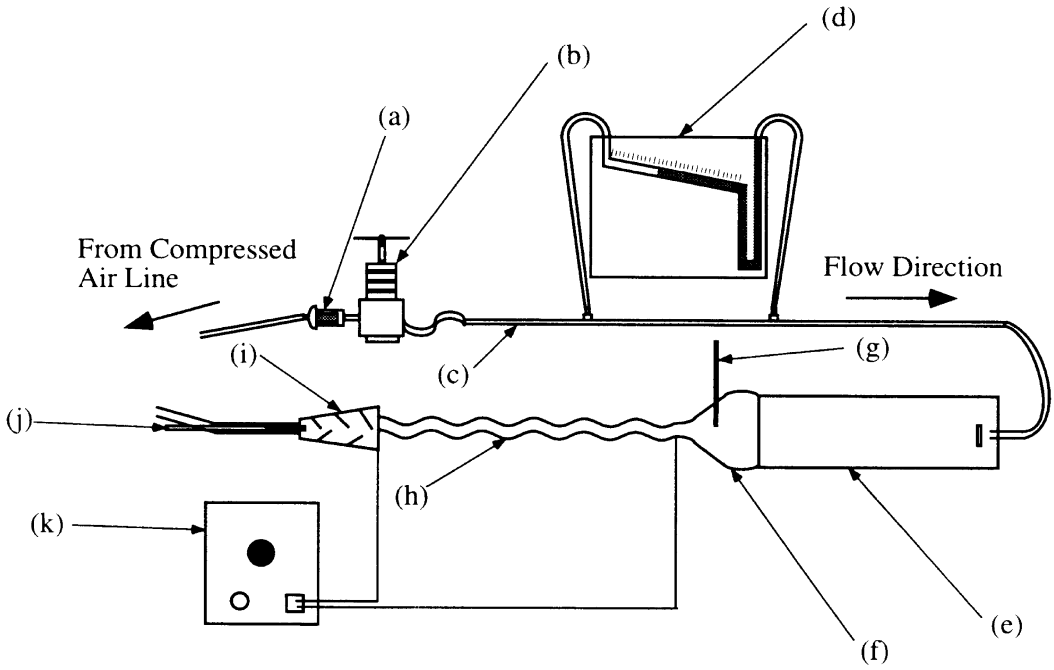

Fig. 3. Schematic of wind tunnel used for heat transfer experiments: (a) supply-air filter; (b) pressure regulator; (c) drawn-copper flow measurement tube; (d) manometer; (e) flow conditioning section with honeycomb and screens; (f) 10 : 1 area contraction; (g) upstream thermometer; (h) test section; (i) downstream mixing station; (j) downstream thermometer; (k) variable transformer, heater control.

inside steel sheet. Thermocouples were placed along the channel centerline at every peak and trough of the wall; two wavelengths had additional thermocouples at 90 and 270°. The greatest source of uncertainty in determining the Nusselt number came from the measurement of the wall temperature, which had an estimated uncertainty of ± 0.25°C. Considering the temperature uncertainties, and uncertainties in flow properties, geometry, and power (heat flux), the average uncertainty in the local heat transfer coefficient was estimated to be $\pm 9.7\%$. The largest uncertainty in the local heat transfer coefficients was $\pm 18.5\%$. The average and largest uncertainties in the local Nusselt number were ± 11.3 and $\pm 20.1\%$, respectively. As with the water tunnel, initially a straight test section was installed in the wind tunnel and the results were compared to the tabular data of Hwang and Fan [25]. Results from the apparatus described above agreed with those of Hwang and Fan to within 12% for the entire test range (Re_D up to 1800, and x^* from 2×10^{-3} to 7×10^{-2}; see [4] for details). As an additional precautionary measure, heat transfer experiments were conducted with the test section installed in several different orientations—accomplished by exchanging the inlet and outlet, and by rotating the test section 90° about the horizontal axis. Test section orientation did not affect the results.

3. Results and discussion

3.1. Flow visualization

Typical flow visualization results for one channel geometry are shown in Fig. 4, where the onset of mixing is plotted as a function of Reynolds number. The flow was deemed 'mixed' when macroscopic mixing between the core fluid and near-wall fluid was manifest, as shown in Fig. 5. Although some judgement was required in determining the wave location of this onset, a relatively clear demarcation was possible by focusing on whether fluid from the steady recirculation zones in the wave troughs was exchanged with core fluid. Repeated experiments demonstrated that, in almost all cases, the demarcation of the mixing onset was determined to within the experimental uncertainty in *Re*. This accuracy is demonstrated in Fig. 4 by the narrow overlap occurring when the onset of mixing moves one wavelength. In Fig. 4, and in the discussion below, the Reynolds number at which the mixing onset jumps from one wavelength to another is called the *transitional Reynolds number*—'transitional' in this case does not necessarily imply turbulence. The first wavelength—counting in the streamwise direction from the inlet—where mixing was observed was taken as the location of the onset of mixing. At very low Reynolds numbers, the flow was steady throughout the channel. At some critical Reynolds number, which depended on the phase shift and other geometric parameters, the flow became unsteady and mixed at a wavelength near the end of the channel. As the Reynolds number increased, the wavelength at which the flow first became mixed moved upstream. Eventually, at a high enough Reynolds number, the flow was unsteady in the first wavelength. These features are captured in the diagram of Fig. 4. All test sections yielded results similar to those shown in Fig. 4—the differences will be discussed below. Furthermore, experiments were conducted by starting at a low *Re* and increasing the flow rate and by starting at a high *Re* and

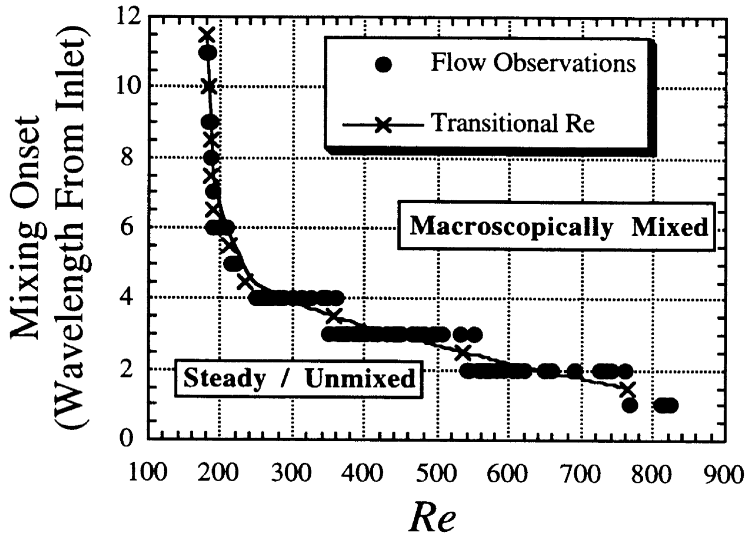

Fig. 4. Typical flow visualization results and example data interpretation. Flows in regions above or to the right of the curve exhibit macroscopic mixing, while flows below and to the left do not. These data are for $\lambda/H_{min} = 4.7$; $A/H_{min} = 0.47$; $\varphi = 0°$.

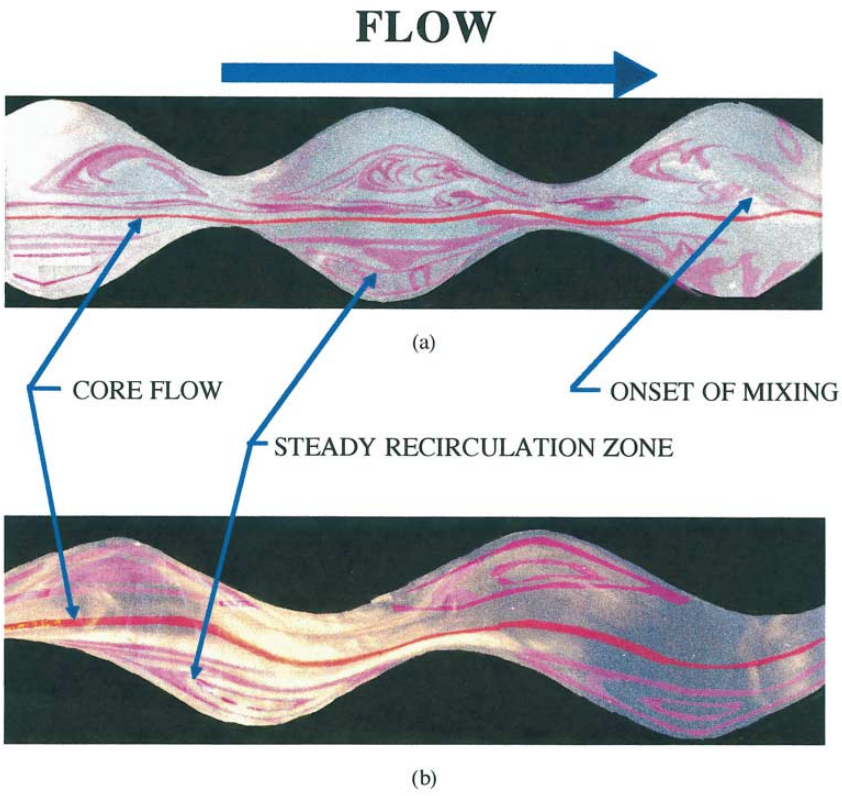

Fig. 5. Typical images from the flow visualization study. Flow for: (a) $Re = 468$; $\varphi = 180^\circ$; $\lambda/H_{min} = 5.6$; $A/H_{min} = 0.48$; (b) $Re = 333$; $\varphi = 90^\circ$, $\lambda/H_{min} = 5.5$; $A/H_{min} = 0.51$.

decreasing the flow rate, and no hysteresis in the results was observed.

The streakline patterns near transition for the $\varphi = 180^\circ$ geometry differed markedly from the patterns observed in the $\varphi = 0^\circ$ and $\varphi = 90^\circ$ test sections, suggesting that different mechanisms are important. When the flow is steady in a $\varphi = 180^\circ$ channel, trapped vortices occupy nearly the entire trough of the wave as shown in Fig. 5a. The onset of mixing is accompanied by small oscillations in the core flow and the formation of roller vortices in the free shear layer. Once roller vortices form and are advected downstream, this shear-layer-driven exchange of fluid results in macroscopic mixing. This process also results in flow three dimensionality, as shown in Fig. 6. Mixing in the $\varphi = 0^\circ$ and 90° channels appears to occur through a different mechanism. When the flow in these channels is steady, the core fluid must turn to pass through the channel. Trapped recirculation zones exist, but they are smaller than in the $\varphi = 180^\circ$ channel, as shown in Fig. 5b. Flow mixing occurs when the core flow undergoes large oscillations, resulting in large changes in the position of the reattachment point of the free shear layer. When the reattachment point moves far enough upstream, the core flow impinging on the wall 'injects' free-stream fluid into the separation bubble; this injection is accompanied by an 'ejection' of fluid from the separation bubble into the core flow. This dynamically driven exchange of fluid results in macroscopic mixing. Three dimensional flow was also observed for the $\varphi = 0^\circ$ and $\varphi = 90^\circ$ channels at the onset of mixing.

Because the overall flow behavior depends strongly on φ, it is not surprising that transitional Reynolds numbers depend strongly on φ. This dependence is shown in Fig. 7, where results are presented for channels with nearly identical values of λ/H_{min} and A/H_{min} but with three different values of φ. The $\varphi = 0^\circ$ and $\varphi = 90^\circ$ channels become unstable at lower Reynolds numbers than the $\varphi = 180^\circ$ channel. This result was found throughout the parameter space of the study; however, for the largest values of A/H_{min}, the transitional Reynolds numbers were only weakly dependent on φ.

The relative wavelength, λ/H_{min}, also affected the transitional Reynolds numbers. For the $\varphi = 180^\circ$ channels, decreasing the wavelength by 20% made the flow less stable—the onset of mixing occurred at lower Re for a fixed position, or nearer the channel entrance for a fixed

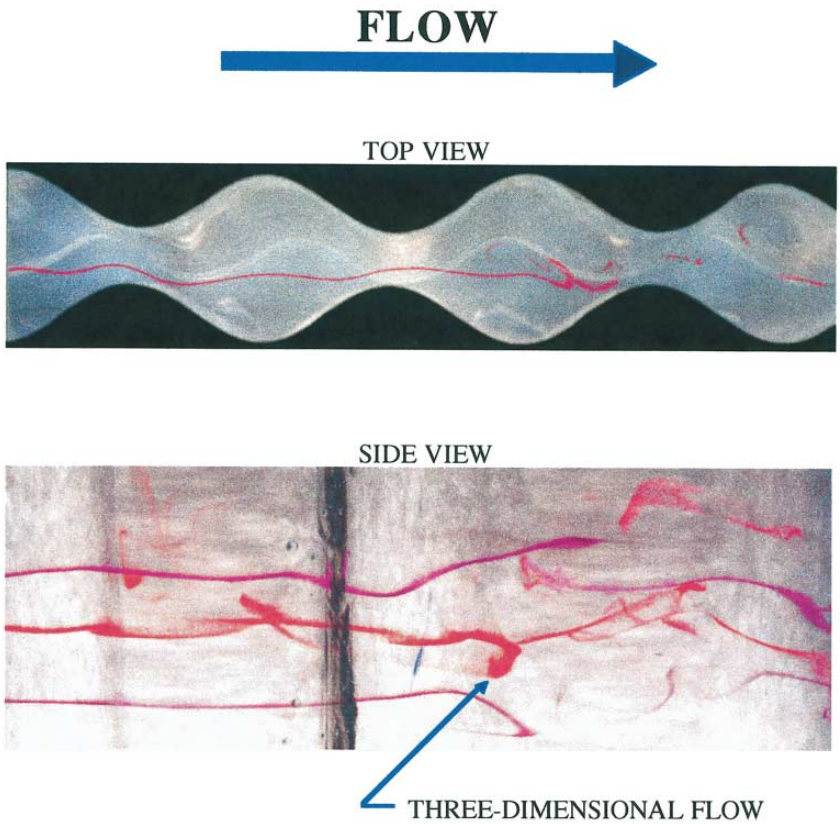

Fig. 6. Flow visualization results showing the onset of mixing and a corresponding change from two- to three-dimensional flow in a wavy passage. $Re = 521$; $\varphi = 180^{\circ}$; $\lambda/H_{min} = 5.6$; $A/H_{min} = 0.48$.

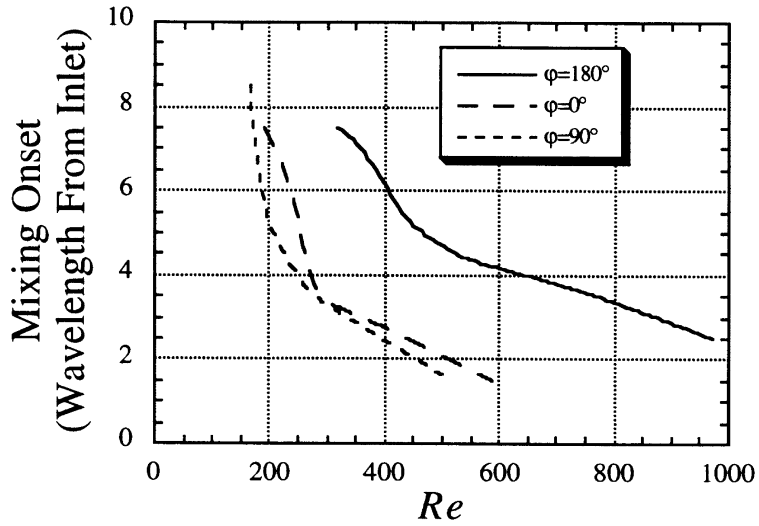

Fig. 7. Typical transitional Reynolds number data for three different phase shifts (φ) at fixed $\lambda/H_{min} = 5.5$ and $A/H_{min} = 0.48$.

Re. These trends were more pronounced for large values of A/H_{min}. For the $\varphi = 0^\circ$ and 90° channels, λ/H_{min} did not significantly influence the onset of mixing; however, increasing the wavelength by 20% had a small stabilizing influence at all values of A/H_{min}. This behavior is shown in the example data provided in Fig. 8, where the effect of relative wavelength on the transitional Reynolds number is quantified.

The effects of A/H_{min} are complex. For all three phase shifts, a large value of A/H_{min} caused an initial onset of mixing to occur at lower Reynolds numbers. As A/H_{min} decreases, the Reynolds number range required for the mixing onset to move from the channel exit to the channel entrance is markedly decreased. This narrower range of transitional Reynolds numbers causes the larger relative-amplitude channel to become unstable in the first wavelength either before or at about the same Reynolds number as a test section with a smaller A/H_{min}. Example data are provided for two different sets of test sections in Fig. 9.

A final noteworthy observation is that the separation zones were very small or nonexistent over the entire Reynolds number range for the channel with $\varphi = 180^\circ$, $\lambda/H_{min} = 2.4$, and $A/H_{min} = 0.26$. There was little evidence of macroscopic mixing in this channel for all Reynolds numbers less than 1000.

3.2. Heat transfer

There are two important factors affecting heat transfer in wavy channels: conventional flow development and wavy-channel effects. Local Nusselt number results for the $\varphi = 0^\circ$ and $\varphi = 180^\circ$ channels are shown in Fig. 10. The heat transfer data are plotted as a function of dimensionless distance from the channel inlet for a range of Reynolds numbers. It is useful to note that the Nusselt number based on plate spacing for fully developed laminar flow in a straight duct is 3.35—with the 10 : 1 aspect ratio taken into account. At low Reynolds numbers, where flow development occurs but macroscopic mixing does not occur, the heat transfer data show that the wavy-channel heat transfer is close to that of the straight duct. This behavior is evident in Fig. 10a at $Re = 108$ and Fig. 10b at $Re = 253$ for the 0 and 180° channels, respectively.

For all Reynolds numbers and all channel geometries, the heat transfer coefficient is high near the channel entrance as clearly demonstrated in Fig. 10. For low Reynolds numbers—below the critical *Re* for the onset of mixing—this effect is solely due to thermal development. At the channel entrance the thermal boundary layer is thinner than under fully developed conditions, and the Nusselt number is therefore higher. If the wavy channels behaved as straight channels, then all the *Nu* data would collapse to a single curve at low *Re*; however, this collapse does not occur because in addition to development effects, wavy-channel heat transfer is influenced by macroscopic mixing in the flow.

The effects of mixing are easiest to discern by examining the Nusselt number behavior near the channel exit for the $\varphi = 0^\circ$ channel. At the lowest Reynolds number of 108, the flow visualization results did not show the presence of mixing; cf Fig. 7. Nevertheless, even at this low Reynolds number, the local Nusselt number increases in the last wave of the channel. This increase is probably due to unsteadiness in the flow that occurs at Reynolds numbers just below the onset of mixing. At $Re = 168$, it

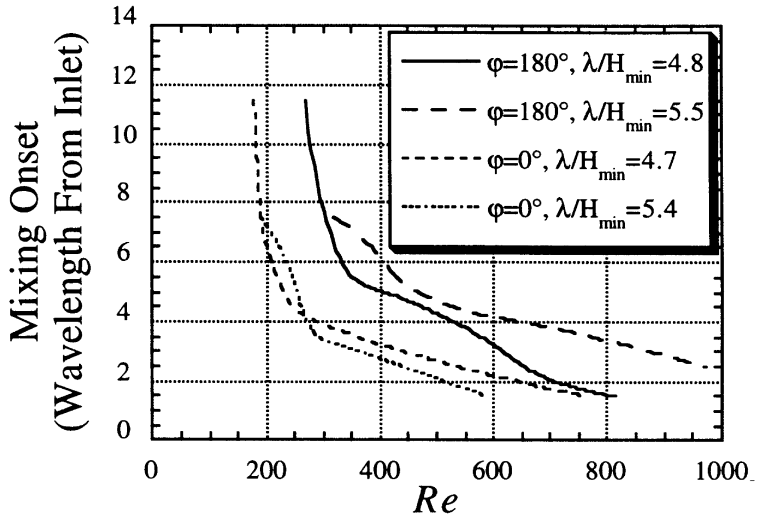

Fig. 8. Typical transitional Reynolds number data for $\varphi = 0^\circ$ with $\lambda/H_{min} = 4.7$ and 5.4; and for $\varphi = 180^\circ$ with $\lambda/H_{min} = 4.8$ and 5.5. For every case shown, $A/H_{min} = 0.48$. These results show the effect of λ/H_{min} at the extreme in φ.

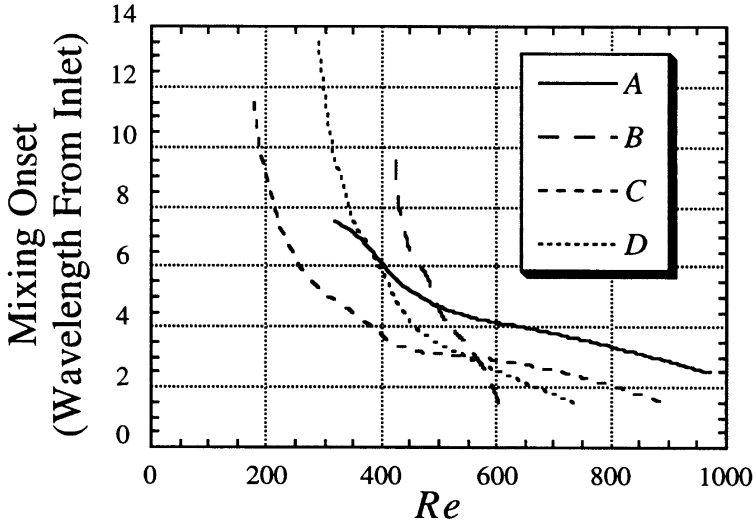

Fig. 9. Typical transitional Reynolds number data for four geometric configurations: (A) $\varphi = 180^\circ$, $A/H_{min} = 0.48$, $\lambda/H_{min} = 5.6$; (B) $\varphi = 180^\circ$, $A/H_{min} = 0.25$, $\lambda/H_{min} = 2.9$; (C) $\varphi = 90^\circ$, $A/H_{min} = 0.52$, $\lambda/H_{min} = 4.9$; and (D) $\varphi = 90^\circ$, $A/H_{min} = 0.24$, $\lambda/H_{min} = 2.3$.

appears as if the last waves in the channel are enhanced through macroscopic mixing; the local Nusselt number shows a sharp increase near the channel exit. As the Reynolds number is increased, the onset of mixing occurs at locations further upstream, and the Nusselt number increases at locations nearer to the channel entrance. At the highest Reynolds number of 788, mixing was evident throughout the channel in the flow visualization studies, and the Nusselt number is increased by mixing throughout the flow length. As a result, the Nusselt numbers are increased even in the developing flow region very near the channel entrance, and the Nusselt number data do not collapse to a single curve; a family of curves in *Re* is required to describe the Nusselt number behavior. It is interesting to compare the $\varphi = 0^\circ$ data of Fig. 10a to the $\varphi = 180^\circ$ data of Fig. 10b. It is difficult to establish the location of the onset of mixing from the local heat transfer data—the location where an enhancement is observed may be slightly upstream or downstream from the onset of mixing. Nevertheless, the general impacts of mixing are the same: mixing enhances heat transfer near the channel exit at low Reynolds numbers (near the first transitional *Re*), and as the Reynolds number is increased, the effects of mixing become important at locations closer to the channel entrances. Above some Reynolds number (~ 600 for $\varphi = 0^\circ$ and ~ 1100 for $\varphi = 180^\circ$), mixing occurs throughout the channel and its impact is important through the entire flow length. At some higher Reynolds number, the flow will become turbulent; however, experiments were not conducted with turbulent flow.

It should be noted that the local Nusselt number data for $Re < 200$ should be considered with caution. At lowest Reynolds numbers, the local Nusselt number uncertainty was high (approximately 20%); at higher Reynolds numbers the uncertainty was lower, and the average *Nu* uncertainty was about 11%, as stated earlier.

4. Conclusions

The heat transfer experiments confirm that instabilities observed in the flow visualization experiments cause a heat transfer enhancement in the wavy channels. This enhancement has been locally quantified in the experiments reported in this paper, and it has been related to the onset of macroscopic mixing. The onset of mixing begins near the channel exit at a relatively low Reynolds number and moves toward the channel entrance as the Reynolds number is increased. The *Nu* enhancement is likewise first manifest near the exit and moves toward the channel entrance with increasing Reynolds numbers.

The flow visualization and heat transfer results provide a basis for the following conclusions:

(1) Even when the approach flow is steady and uniform, flow is unsteady and unstable in wavy channels in the laminar flow regime. Unsteadiness first appears at the end of the channel and eventually moves upstream to the first wavelength with increasing Reynolds number.
(2) In the $\varphi = 180^\circ$ geometries, the flow separates from the channel walls at very low Reynolds numbers and vortices are trapped in the troughs of the channel when the flow is steady. The flow becomes unsteady

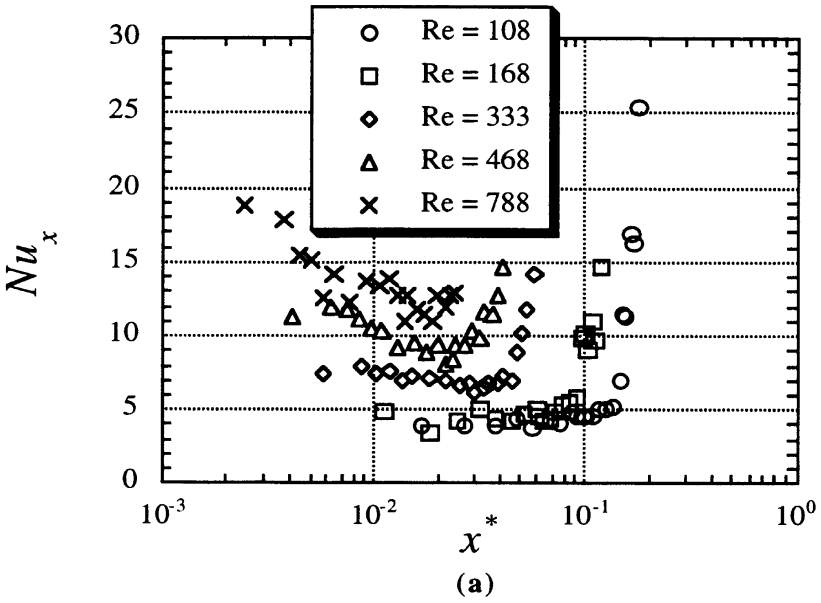

(a)

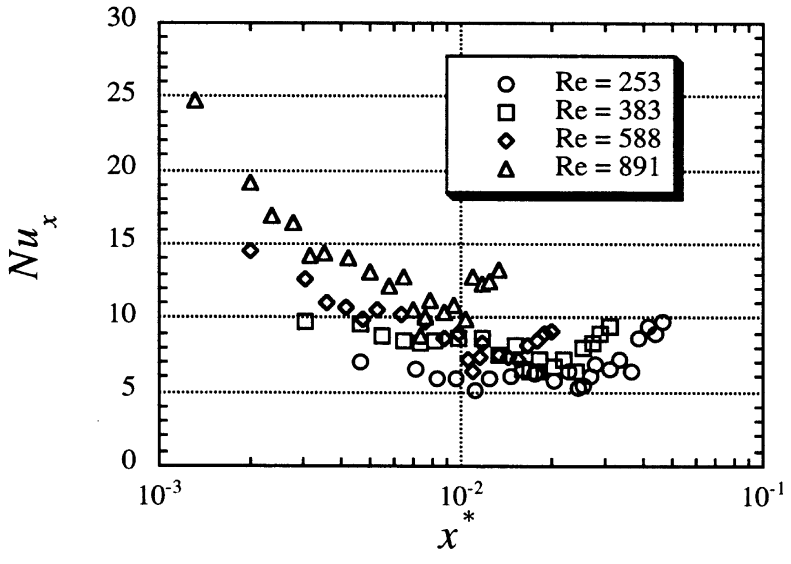

(b)

Fig. 10. Local Nusselt number, Nu_x, vs $x^* = x/(H_{min}Re)$ for: (a) $\varphi = 0^\circ$, $A/H_{min} = 0.5$, and $\lambda/H_{min} = 5.5$; and (b) $\varphi = 180^\circ$, $A/H_{min} = 0.5$, and $\lambda/H_{min} = 5.5$, for a family of Reynolds numbers.

when the shear layer between the trapped vortices and the core fluid becomes unstable.

(3) In the $\varphi = 0^\circ$ and $\varphi = 90^\circ$ geometries, the flow also separates from the channel walls at very low Reynolds numbers and standing vortices form in the channel. Macroscopic mixing occurs when the oscillating reattachment point moves upstream and the impinging flow 'injects' fluid into the trapped vortex.

(4) Phase shift plays an important role in the stability of the channel flow. For a given Reynolds number, the

$\varphi = 0^\circ$ and $\varphi = 90^\circ$ geometries are unsteady farther upstream than the $\varphi = 180^\circ$ geometry.

(5) In the range of parameter space studied (λ/H_{min} between 2.3 and 5.6), relative wavelength, λ/H_{min} did not significantly influence the onset of mixing in the wavy passage.

(6) Relative amplitude, A/H_{min} plays an important role in the stability of the wavy channel at low Reynolds numbers. A larger relative amplitude delays the initial onset of instability in the channel. At higher *Re*, the effect of relative amplitude diminishes significantly.

(7) There is a heat transfer enhancement due to the geometry of the wavy passage for laminar flow. The location of the onset of this heat transfer enhancement is a function of Reynolds number; as the Reynolds number is increased the location of wavy-channel heat transfer enhancement moves closer to the entrance of the channel.

(8) At high enough Reynolds numbers to move the location of the onset of unsteadiness near the entrance of the channel, the heat transfer enhancement due to the geometry of the wavy channel augments the enhancement due to normal development effects.

The parameter space in wavy-channel flows is extensive and needs to be explored more thoroughly before an optimum geometry for specific conditions can be determined. Furthermore, pressure-drop data were not recorded in this study, and such data are needed to determine the overall thermal benefit of a particular wavy channel in a specified application. It may be desirable to undertake thermal performance testing of wavy channel heat exchangers in full-scale experiments—such experiments are needed to account for the geometrical complications, manufacturing, water retention, frosting, and fouling effects commonly encountered in application.

Acknowledgements

The authors gratefully acknowledge support from the Air Conditioning and Refrigeration Center (ACRC) at the University of Illinois. The ACRC is an NSF Industry–University Cooperative Research Center.

References

[1] A.M. Jacobi, R.K. Shah, Air-side flow and heat transfer in compact heat exchangers: a discussion of enhancement mechanisms, Heat Transfer Engineering 9 (1998) 29–41.

[2] K. Stone, Numerical study of flow and heat transfer in wavy passages, MS Thesis, University of Illinois at Urbana-Champaign, 1997.

[3] S. Vȍelker, S.P. Vanka, Fluid Flow and Heat Transfer in Serpentine Channels at Low Reynolds Numbers, Air Conditioning and Refrigeration Center ACRC TR-115, University of Illinois at Urbana-Champaign, 1997.

[4] T.A. Rush, An Experimental Study of Flow and Heat Transfer in Wavy Passages, MS Thesis, University of Illinois at Urbana-Champaign, 1997.

[5] J.L. Goldstein, E.M. Sparrow, Heat mass transfer characteristics for flow in a corrugated wall channel, Journal of Heat Transfer 99 (1977) 187–195.

[6] J.E. O'Brien, E.M. Sparrow, Corrugated-duct heat transfer, pressure drop, and flow visualization, Journal of Heat Transfer 104 (1982) 410–416.

[7] E.M. Sparrow, J.W. Comb, Effect of interwall spacing and fluid flow inlet conditions on a corrugated-wall heat exchanger, International Journal of Heat and Mass Transfer 26 (1983) 993–1005.

[8] R.S. Amano, A. Bagherlee, R.J. Smith, T.G. Niess, Turbulent heat transfer in corrugated-wall channels with and without fins, Journal of Heat Transfer 109 (1987) 62–67.

[9] Y. Asako, M. Faghri, Finite-volume solutions for laminar flow and heat transfer in a corrugated duct, Journal of Heat Transfer 109 (1987) 627–634.

[10] M. Ali, S. Ramadhyani, Experiments on convective heat transfer in corrugated channels, Experimental Heat Transfer 5 (1992) 175–193.

[11] J.M. Choi, N.K. Anand, S.C. Lau, R.T. Kureja, Heat (mass) transfer in a serpentine channel with right-angled turns, Journal of Heat Transfer 118 (1996) 211–213.

[12] T. Nishimura, Y. Kajimoto, A Tarumoto, Y. Kawamura, Flow structure and mass transfer for a wavy channel in transitional flow regime, Journal of Chemical Engineering Japan 19 (1986) 449–455.

[13] T. Nishimura, T. Yoshino, Y. Kawamura, Instability of flow in a sinusoidal wavy channel with narrow spacing, Journal of Chemical Engineering Japan 20 (1987) 102–104.

[14] T. Nishimura, K. Yano, T. Yoshino, Y. Kawamura, Occurrence and structure of Taylor–Goertler vortices induced in two-dimensional wavy channels for steady flow, Journal of Chemical Engineering Japan 23 (1990) 697–703.

[15] Y. Asako, H. Nakamura, M. Faghri, Heat transfer and pressure drop characteristics in a corrugated duct with rounded corners, International Journal of Heat and Mass Transfer 31 (1988) 1237–1245.

[16] V.K. Garg, P.K. Maji, Flow and heat transfer in a sinusoidally curved channel, International Journal of Engineering Fluid Mechanics 1 (1988) 293–319.

[17] T. Nishimura, Y. Ohori, Y. Kawamura, Flow characteristics in a channel with a symmetric wavy wall for steady flow, Journal of Chemical Engineering Japan 17 (1984) 466–471.

[18] T. Nishimura, Y. Ohori, Y. Kajimoto, Y. Kawamura, Mass transfer characteristics in a channel with symmetric wavy wall for steady flow, Journal of Chemical Engineering Japan 18 (1985) 550–555.

[19] T. Nishimura, A. Tarumoto, Y. Kawamura, Flow and mass transfer characteristics in wavy channels for oscillatory flow, International Journal of Heat and Mass Transfer 30 (1987) 1007–1015.

[20] T. Nishimura, S. Murakami, S. Arakawa, Y. Kawamura, Flow observations and mass transfer characteristics in sym-

metrical wavy-walled channels at moderate Reynolds numbers for steady flow, International Journal of Heat and Mass Transfer 33 (1990) 843–845.
[21] A.M. Guzmán, C.H. Amon, Transition to chaos in converging-diverging channel flows: Ruelle–Takens–Newhouse scenario, Physics of Fluids 6 (1994) 1994–2002.
[22] A.M. Guzmán, C.H. Amon, Dynamical flow characterization of transitional and chaotic regimes in converging–diverging channels, Journal of Fluid Mechanics 321 (1996) 25–57.
[23] G. Wang, S.P. Vanka, Convective heat transfer in periodic wavy passages, International Journal of Heat and Mass Transfer 38 (1995) 3219–3230.
[24] N. Saniei, S. Dini, Heat transfer characteristics in a wavy-walled channel, Journal of Heat Transfer 115 (1993) 788–792.
[25] G. Tanda, G. Vittori, Fluid flow and heat transfer in a two-dimensional wavy channel, Warme- und Stoffubertragung 31 (6) (1996) 411–418.
[26] B. Snyder, K.T. Li, R.A. Wirtz, Heat transfer enhancement in a serpentine channel, International Journal of Heat and Mass Transfer 36 (1993) 2965–2976.
[27] F.M. White, Fluid Mechanics, 2nd ed., McGraw-Hill, New York, 1986.
[28] C.L. Hwang, L.T. Fan, Finite difference analysis of forced convection heat transfer in entrance region of a flat rectangular duct, Applied Scientific Research, A13 (1964) 401–422.